MICROMECHANICAL MODELLING AND INTERFACIAL STRENGTH PREDICTION OF MULTIDIRECTIONAL LAMINATED FIBRE REINFORCED POLYMERS

Ákos Bolyky[1], Ioannis K Giannopoulos[1*], Efstathios E Theotokoglou[2]

[1]*Centre of Excellence for Aeronautics, School of Aerospace, Transport and Manufacturing, Cranfield University, Cranfield, MK43 0AL, UK*

[2] *Department of Mechanics, Laboratory of Testing and Materials, School of Applied Mathematical and Physical Sciences, National Technical University of Athens, GR-157 73, Greece*

Abstract: Delamination initiation and propagation is a common failure mode in laminated composites that must be considered when assessing damage in composite structures. Delamination usually propagates at the interface between laminas. Current approved testing procedures address the inter-laminar strength in fracture modes I and II for interfaces of unidirectional laminas oriented in the same direction. The aim of this study was to investigate the inter-laminar fracture initiation strength in multi-layer lamina interfaces by the use of micromechanical numerical analysis. Representative volumetric elements with randomly distributed fibres and the ability of numerically modelling fibre-matrix interfacial de-bonding were generated with different ply interfacial orientations. Failure initiation and damage sequences were captured and the global stresses where failure initiated were determined for the studied configurations. Insights on the variations in the strength observed due to the different lamina orientations were provided.

1. Introduction

Fibre reinforced polymer composite materials (FRPs) have been extensively applied to structures with increased performance needs in terms of specific strength and stiffness. For these structurally demanding applications, FRPs constitute mostly of pre-impregnated (pre-preg) toughened epoxy matrices reinforced with unidirectional (UD) long carbon fibres (CFRPs) and are supplied in the form of thin laminas of a few tenths of a millimeter in thickness. These laminas are stacked up and directionally tailored to form thicker laminates of several millimeters in order to meet the required design criteria and performance.

Due to the nature of the supplied FPR material, the processing methods and the in-service loading, a very common failure mode observed laminated FRPs is delamination in the forms of intra-ply cracks and inter-laminar splits. Intra-ply delamination is the material separation within a lamina, and inter-laminar delamination is the separation between the individual laminas in a laminate stack. The laminated material can split into its separate laminas under the three well known modes; opening mode I, shearing mode II and scissoring mode III, the first two of them are depicted in figure 1.

The research question in regards to the load needed for initiating damage in any of the above mentioned modes of material failure as well as the energy needed to be consumed for the damage propagation along the interface has been partially addressed by the research and engineering community in the field of study. Currently, validated testing methods exist for describing the interfacial strength and fracture energy for initiating and propagating a crack in modes I and II, between laminas of the same unidirectional orientation. To this date, a validated testing procedure for interrogating these quantities for interfaces between laminas of different orientations does not exist.

---

[*] Corresponding author
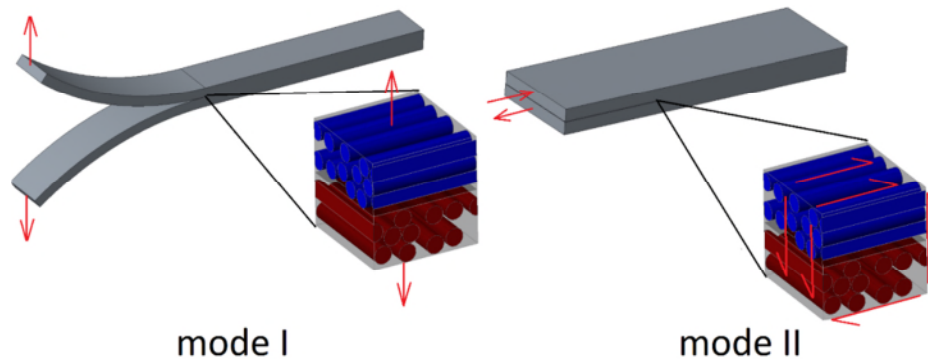E-mail address: i.giannopoulos@cranfield.ac.uk

Figure 1: Unit cell and loading for mode I and mode II delamination between 0° and 90° plies

The aim of the work presented herein, was to investigate the failure initiation strength in a multidirectional stack of unidirectional laminas and the differences occurring in the case of various layup arrangements by the use of micromechanical numerical analysis.

2. Micromechanical analyses and Representative Volumetric Elements (RVE)

Micromechanical analyses of fibre reinforced polymer composite materials are making use of Representative Volumetric Elements (RVEs) which model only a representative part of the microstructure. In elasticity problems they have been used for the derivation of closed form displacement field solutions. The assumption underlining the usage of the RVEs is that the mechanical response of the material macroscopically can be pieced together following the response in the repetitive pattern of the representative volume modelled.

Ruled fibre array RVEs which assume equal spacing between each fibre inside the matrix material, are simplifying reality where fibres are randomly distributed inside the matrix. The fibre density varies and pockets of resin-rich areas appear similarly to increased fibre density. Researchers have started to use randomly distributed arrays of fibres for better representing the mechanical properties distributions and for capturing the damage initiation and propagation and the failure mechanisms involved. McCarthy and Vaughan [1] investigated the variation on the interfacial traction and the stress variation between the fibre and matrix contact surfaces. In their research they showed that the effects of fibre array and the relative proximity of the fibres within the matrix is very crucial for fibre-matrix de-bonding and influences the stress state inside the matrix. The same authors presented a technique for generating statistically equivalent fibre distributions for high volume fraction composite materials [2] approach called the Nearest Neighbour Algorithm (NNA).

Trias et al. [3] investigated the critical size of a statistical RVE for CFRP materials. In their study, they analysed several criteria to define the minimal required size of the RVE. Each of these criteria was satisfied with different model sizes, and the maximum of these values defines the minimum size for a statistical RVE. According to their results, the coefficient of variation is the most demanding criterion, for which the required minimal size of the RVE was $L = 50R$, where L is the length of the element side and R is the fibre radius.

Llorca and González [4] investigated the ideal RVE size. They found that a unit cell with 30 fibres is good enough to represent the FRP material in their study. O'Dwyer et al. [5] used an edge length of $L = 40 \, \mu m$ for the investigation of the same material as used in the present study. They stated that this RVE size is comparable to those of similar three-dimensional studies and that an increase of this has negligible effect on the results. For the present work, the RVE edge length of $L = 40 \, \mu m$ also showed a good compromise between model accuracy and computational costs.

3. Numerical model generation

A unidirectional fibre reinforced polymer material was modelled micromechanically, shown in figure 2. The material comprised of carbon fibres reinforcing the epoxy matrix resin, with a 59% fibre volume fraction and having fibre diameters (D) of 6.6μm. Random array RVEs were generated using a commercial multi-scale material modelling software DIGIMAT® [6] in three different orientation layouts 0°/0°, 0°/90° and 0°/45°.

a)   b)   c)
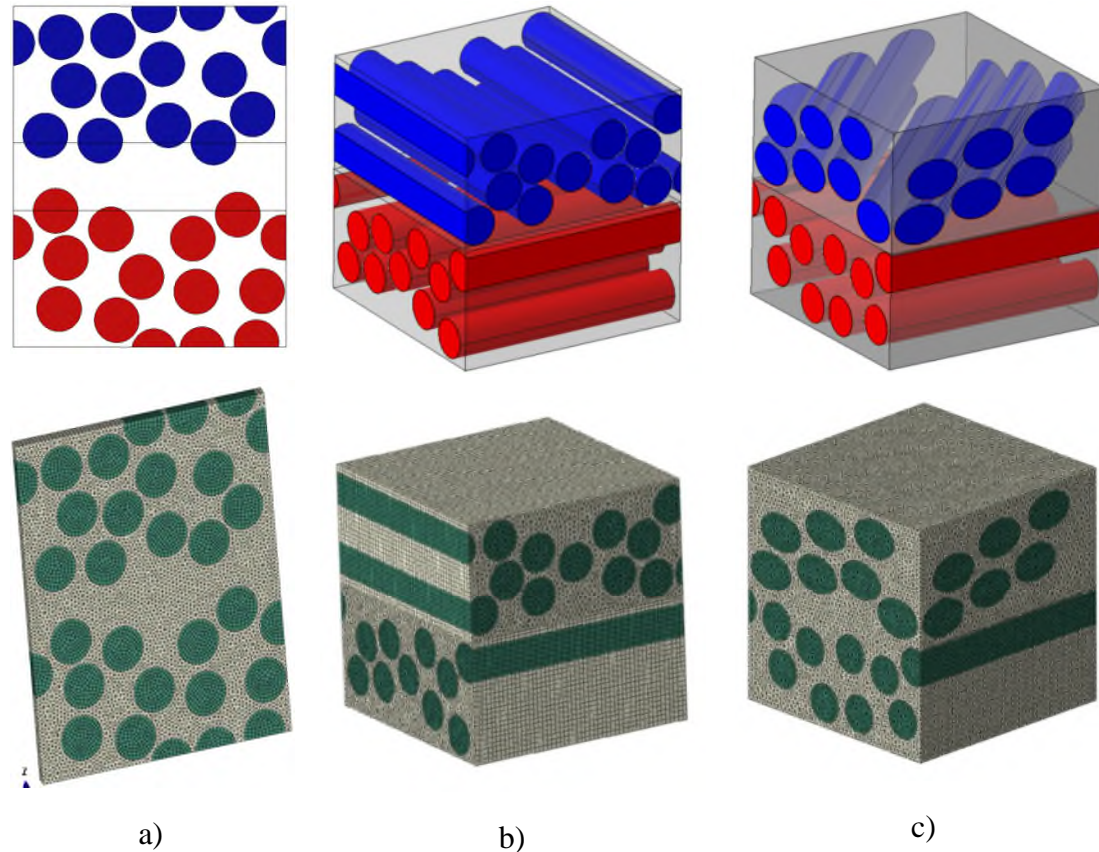
Figure 2: Micromechanical random array RVEs with different lamina orientations a) 0°/0°, b) 0°/90° and c) 0°/45° for investigating the damage initiation strength

In order to ensure adequate discretisation and avoid distorted elements, during the random generation process, fibre gap between neighbouring fibres was larger than 0.035 x D and the volume of the sectioned fibres at the edges of the RVE were at least one tenth of the volume of a whole fibre. For each model, a Python script was exported and processed in ABAQUS® [7]. Quadratic shape function triangular prism elements (C3D15) and brick elements with reduced integration (C3D20R) were used for the discretization of the matrix and fibre material respectively. The interface between the fibres and the matrix was modelled with cohesive surface bilinear traction separation displacement relations. The cubic RVE sizes shown in figure 2b and 2c were 40 x 40 x 40 μm in size while the RVE which represented the same fibre orientation in its two layers shown in figure 2a was limited to a few micrometres in width. In the case of long-fibre-reinforced composites manufactured by pre-preg technology, a resin-rich area can be observed between each layer [8]. To account for that, a third layer was built in between the two composite laminas in each RVE. This layer was assumed to have a thickness of 10 μm.

Periodic Boundary Conditions (PBCs)

To ensure continuity between neighbouring RVEs and that the stress field inside the model behaves as it was part of a whole structure, periodic boundary conditions were applied. The process of fibre random generations was performed in away such that opposite edges contained supplementary fibres and that displacement across opposite edges remained constant. The effect of PBC application in the shear deformation on the unidirectional laminate is shown on figure 3.
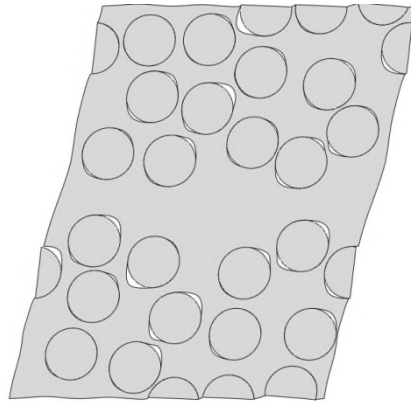

Figure 3: Periodic boundary conditions on the shear response of and RVE, showing the affinity in the displacements of adjacent boundaries

Loading

Three reference points at three perpendicular faces of each RVEs were created. These points were connected to the RVE faces by several multi-point constraints. Boundary conditions and loads were directly defined on these reference points as displacement constraints.
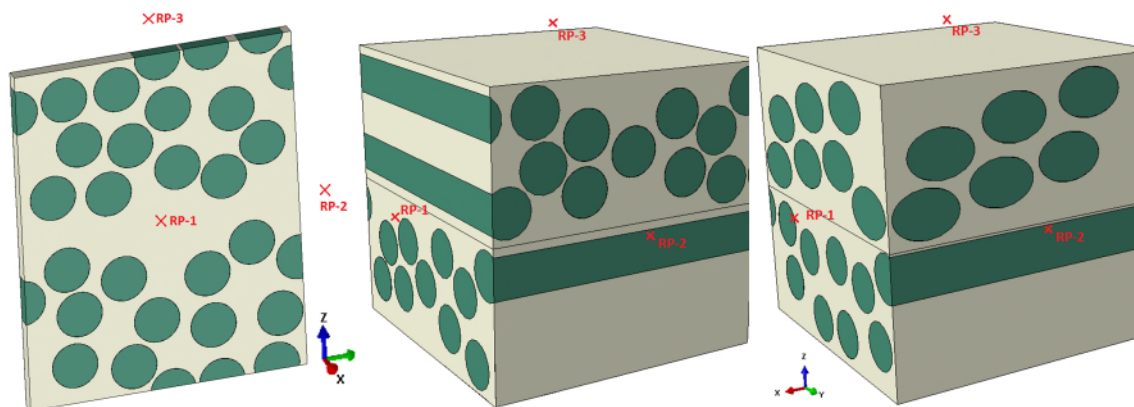

Figure 4: Points related to the RVE faces, were displacement input and reaction load output was controlled

Three loading cases were considered for the unidirectional RVE, shown in figure 5 a), b) and c). Displacements were applied to represent opening and shear delamination of the

0°/0° layout, shown in figure 5 a) and b). For the same RVE shear deformation was also applied to determine mode II strength between two plies oriented in 90°/90°, shown in figure 5c). Similarly, three loading cases were defined for the 0°/90° shown in figure 5d), e) and f) and the 0°/45° shown in figure 5g), h) and i). The shearing case shown in figures 5f) and 5i) were considered for investigating mode II strength between two plies oriented in ±45° and 90°/45° respectively.
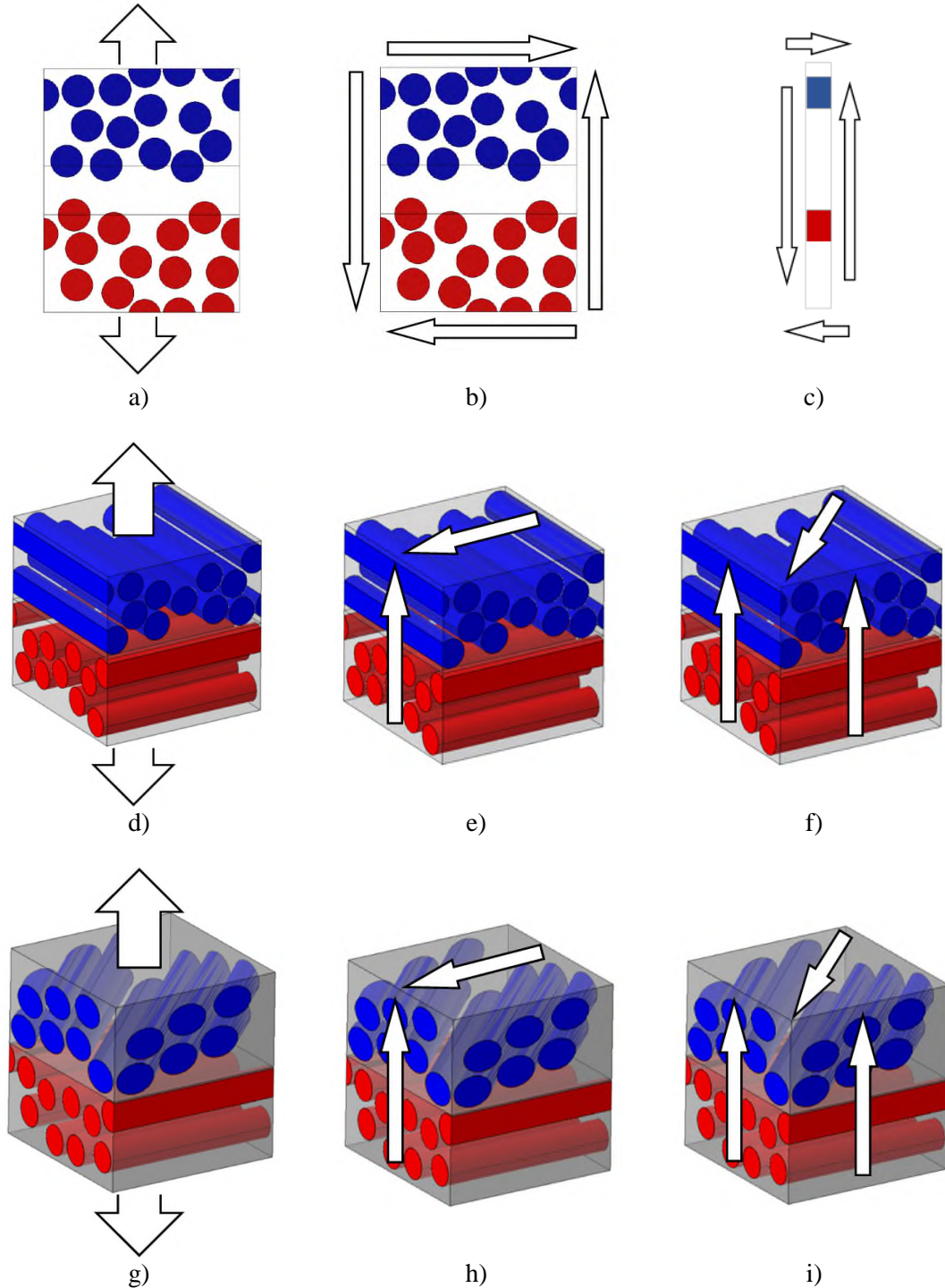

Figure 5: Multidirectional RVEs along with their respective loading scenarios

Material modelling

The damage initiation failures were focused on the matrix plastic failure and the interface cohesive failure between the matrix and the fibre. Under the assumed tensile and shear loading scenarios, fibre fracture was not expected hence fibre failure was not modelled. In that regards, fibres were modelled as having linear elastic behaviour and were assumed without any damage. The elastic behaviour of the fibres was defined by a transversely orthotropic material model. The elastic constants are listed in Table 1.

Table 1: Elastic properties of HTA fibres [9]

Modulus of Elasticity along the fibre direction	E_{11} (MPa)	238000
Modulus of Elasticity transverse to the fibre direction	E_{22} (MPa)	28000
Modulus of Elasticity transverse to the fibre direction	E_{33} (MPa)	28000
Poisson's ratio	ν_{12}	0.23
Poisson's ratio	ν_{23}	0.33
Poisson's ratio	ν_{31}	0.03
Shear Modulus of Elasticity	G_{12} (MPa)	24000
Shear Modulus of Elasticity	G_{23} (MPa)	7200
Shear Modulus of Elasticity	G_{31} (MPa)	24000

For the constitutive modelling of the epoxy resin matrix, Vaughan and McCarthy [9] used a material model with Mohr-Coulomb plasticity introduced by Llorca et al. [4]. This material modelling assumption was found to accurately capture the shear stress dependent yield behaviour of epoxies. During the present investigation it was experienced that implementing the Mohr-Coulomb plasticity, besides its extremely high computational requirements, it generated numerous convergence problems to the solution. Experimenting with various numerical computational schemes, it was discovered that explicit numerical algorithms with this type of plasticity modelling proved to be more stable than their implicit equivalents. Due to the specific nature of the boundary conditions applied which are described on the following sections and were not supported by the explicit scheme, the implicit solver was used and the matrix was modelled as a linear elastic material. The matrix principle stress levels were monitored and failure was assumed upon reaching the peak strength values under tension or compression. The material properties of the epoxy resin are taken from reference [9] and are shown on table 2.

Table 2: Elastic properties of 6376 epoxy resin [9]

Modulus of Elasticity	E (MPa)	3630
Poisson's ratio	ν	0.34
Tensile strength	σ_t (MPa)	103
Compressive strength	σ_c (MPa)	264

In regards to the interface modelling, unidirectional fibre reinforced polymers when subjected to loading along the transverse direction in respect to the fibre direction, damage usually initiates at the fibre-matrix interface which leads to matrix cracking. To account for this effect, interface de-bonding between the matrix and fibres was built in the model.

Cohesive zone modelling (CZM) technique was used, where cohesive behaviour was defined by a bilinear traction-separation law between the two surfaces in contact, i.e. the surface of the fibres and the annular surface of the matrix surrounding the fibres. Surface-based CZM modelling technique was used and zero interface thickness was assumed for this study. Surface-based cohesive behaviour is a simplified way of cohesive elements, which is only applicable for the case of zero interface thickness.

For the bilinear traction-separation laws in the cohesive surfaces, the initial stiffness, the peak stress and the critical strain energy release rate for each separation mode were found in the work of Camanho et al. [10]. Following that work, the initial stiffness for each modes was set to maintain continuity of the stress and strain fields between the fibres and matrix. Mode I and mode II cohesive strength and critical strain energy release rate values were taken from [9] while the mode III parameters were assumed to be equal to those of mode II. O'Dwyer et al. [5] showed that these parameters provide good correlation to experimental observations.

Mode-dependent cohesive surfaces were defined with the ability to account for mixed-mode separation. Damage initiation under mixed-mode conditions was defined by the quadratic stress criterion. Mixed-mode behaviour of damage evolution was defined by the BK law [11]. The mixed-mode interaction parameter used in the BK equation was assumed to equal to 1.45, similarly as in [10]. The parameters which define the fibre-matrix interface are summarised in Table 3.

Table 3: Fibre-matrix interface properties [9, 10]

Traction separation law initial stiffness for fracture mode I	K_I (N/mm^3)	10^8
Traction separation law initial stiffness for fracture mode II	K_{II} (N/mm^3)	10^8
Traction separation law initial stiffness for fracture mode III	K_{III} (N/mm^3)	10^8
Traction separation law peak stress for fracture mode I	t_I^0 (MPa)	85
Traction separation law peak stress for fracture mode II	t_{II}^0 (MPa)	125
Traction separation law peak stress for fracture mode III	t_{III}^0 (MPa)	125
Critical strain energy release rate for fracture mode I	G_{IC} (N/mm)	0.01
Critical strain energy release rate for fracture mode II	G_{IIC} (N/mm)	0.025
Critical strain energy release rate for fracture mode III	G_{IIIC} (N/mm)	0.025
B / K mixed mode fracture propagation law coefficient	η (-)	1.45
Nonlinear simulation numerical viscosity parameter	(-)	$2\text{x}10^{-4}$

The use of cohesive zone modelling often introduces instability and convergence issues in the model. To account for this effect, viscous stabilisation of the damage variable was applied. Stabilisation is defined by a viscosity parameter, which limits the amount of change in the damage variable throughout one analysis time increment. It was found that for the current study, a viscosity parameter of $2\text{x}10^{-4}$ was enough for obtaining stable convergence, but still small enough not to introduce inaccuracy to the model. The same value was used by O'Dwyer et al. in [5].

4. Results and discussion

The micromechanical models generated and shown in figure 2, were loaded in tension perpendicular to the fibre direction for representing mode I fracture initiation as well as in shear for representing mode II under all possible directional orientations, as depicted in figure 5. Representative figures of the results are presented in figures 6 through 12 and further insights to these are discussed further below.
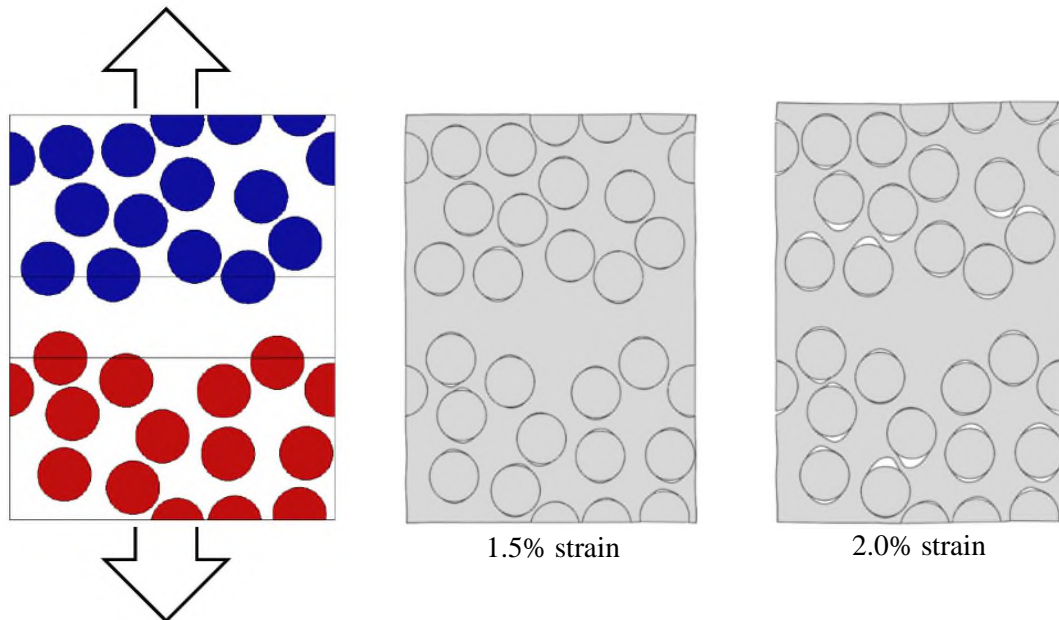

1.5% strain   2.0% strain

Figure 6: Loading scenario and scaled deformed shape of 0°/ 0° laminate in tension, showing the failed cohesive interfaces

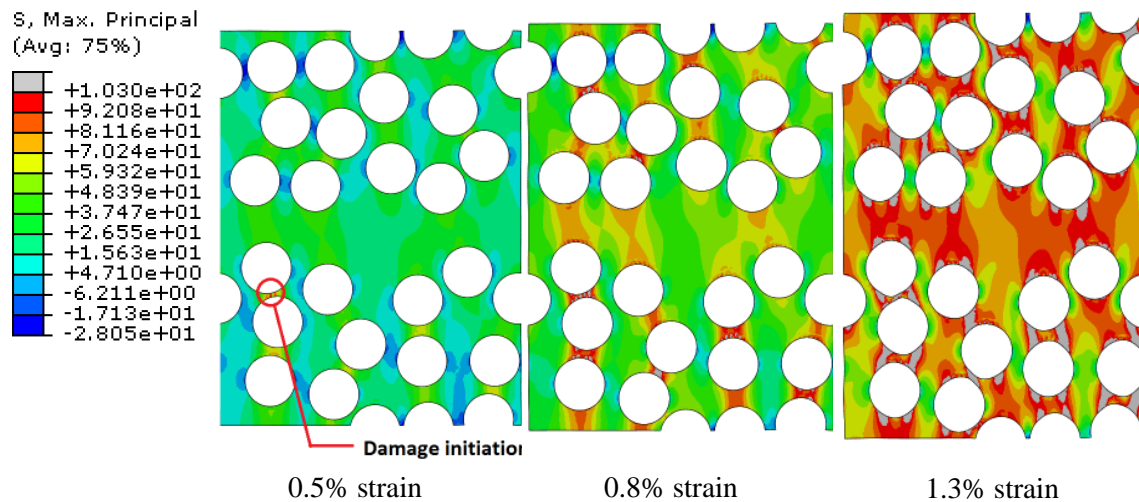0.5% strain   0.8% strain   1.3% strain

Figure 7: Maximum principle stress fringe plot of the 0°/0° laminate in tension, indicating the location of matrix damage initiation at 0.5% tension strain

For the unidirectional RVE loaded in tension shown in figure 6, it was found that fibre-matrix cohesive interface damage initiation started at a lower load than matrix yield initiation. The first interfacial cohesive de-bonding initiated at around 0.5% of the global strain and some fibre-matrix cohesive interfaces failed completely when the strain reached

2.0% as shown in figure 6. In agreement with the experimental observations, damage under such loading, initiates at fibre-matrix interfaces and the cracks formed propagate into the matrix. Maximum principal tensile stress inside the resin first reached the epoxy matrix tensile strength equal to 103 MPa at a thin portion of the matrix between two fibres with relatively close proximity which had partially failed cohesive interfaces. It was also observed similarly to the first damage initiation point that maximum principal stress reached high values between fibres with close proximity. The stress plots after the principal stress first reached the tensile strength do not represent the real stress-state of the matrix since the material model was linear-elastic material model disregarding material deformation due to yielding and free surface generation due to matrix cracking.

For the same unidirectional RVE under the mode II loading scenario shown in figure 8, similar observations were made with the previous case. It was observed that the maximum principal stress inside the matrix reached its peak value at the same location as in the case of tensile loading. Damage initiation of fibre-matrix interfaces was also observed before matrix damage occurred. However, unlike in case of tension, there were no completely failed cohesive interfaces until the point where yield was initiated in the matrix.
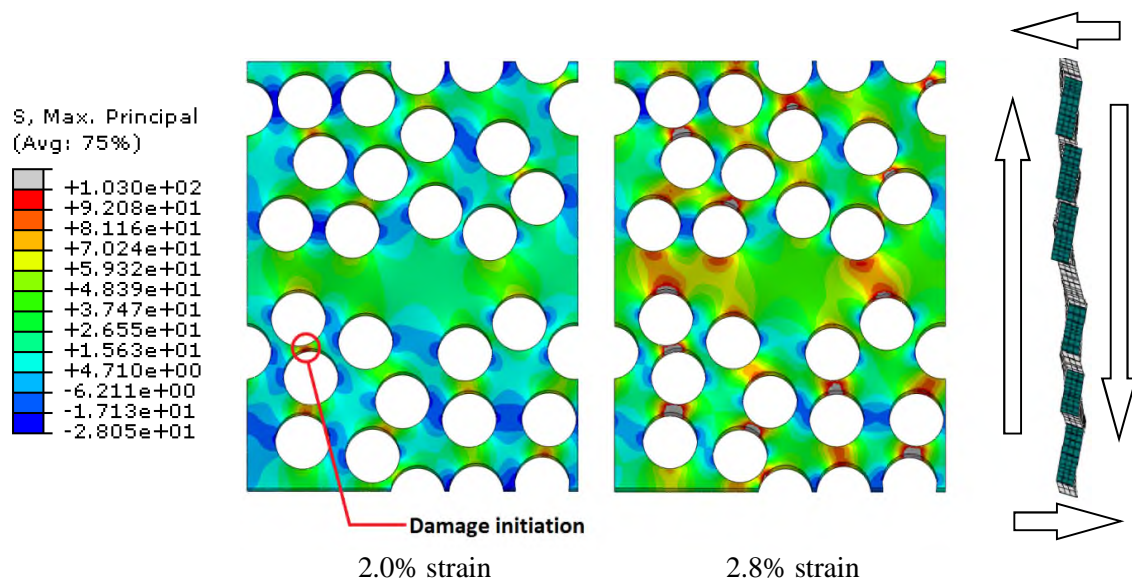

Figure 8: Maximum principle stress fringe plot and the deformed shape of the 0°/0° laminate in mode II shear loading, indicating the location of damage initiation at 2.0% shear strain

The same unidirectional RVE under the loading condition shown in figure 9, represented the mode II case between two 90°/90° laminas. The maximum principal stress plots of this scenario are shown in figure 10. Similarly to the previous cases, failure inside the matrix occurred between two fibres situated in a relatively small distance to each other.

Another observation was that neighboring fibres were connected by a high-stress area of approximately 45° angle to the horizontal reference, which agrees with observations in composites under transverse shear. Similarly to the case of the 0°/0° laminate under shearing, stiffness degradation in some fibre-matrix interfaces can be observed before matrix damage, but complete cohesive de-bonding did not occur prior to matrix yield.
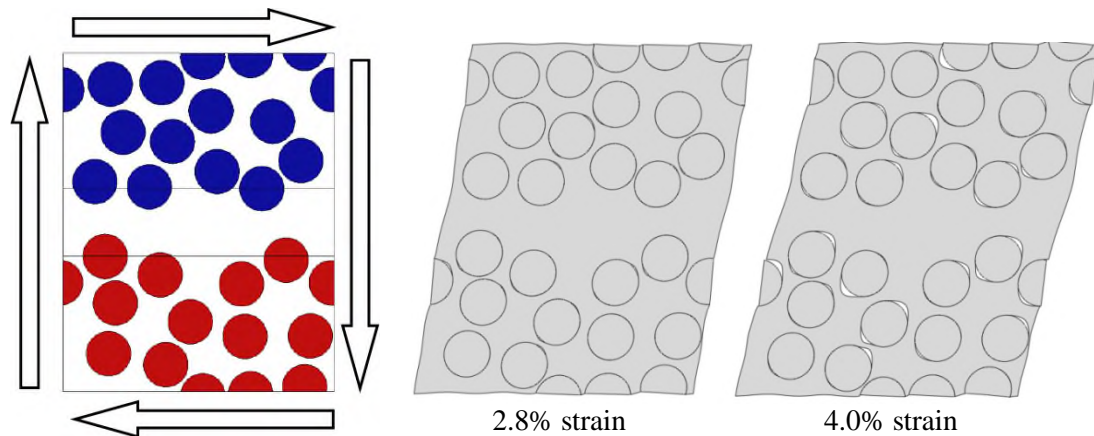

2.8% strain   4.0% strain

Figure 9: Loading scenario and scaled deformed shape of 90°/ 90° laminate in shear, showing the failed cohesive interfaces
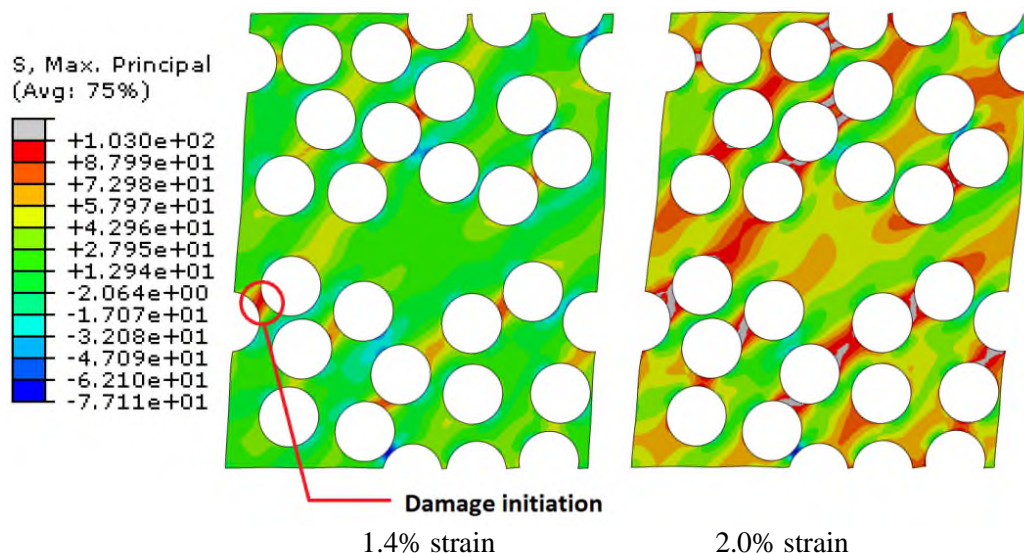

1.4% strain   2.0% strain

Figure 10: Maximum principle stress fringe plot superimposed on the deformed shape of the 90°/ 90° laminate in shear, indicating the location of damage initiation at 1.4% shear strain

Similarly to the previous analyses, figure 11 depicts the 0°/90° RVE under tensile loading. The deformed shape under tension showed that cohesive interface de-bonding occurred in both laminas. Stiffness degradation of several fibre-matrix interfaces was observed which influenced the stress field inside the matrix. Figure 12 shows the maximum principal stress fringe plots with the fibres being removed from the model. Yield failure inside the resin initiated in the upper ply due to the closer proximity in the fibre arrangement. As before, damage was located at a high-stress area between two fibres with damaged cohesive interfaces.
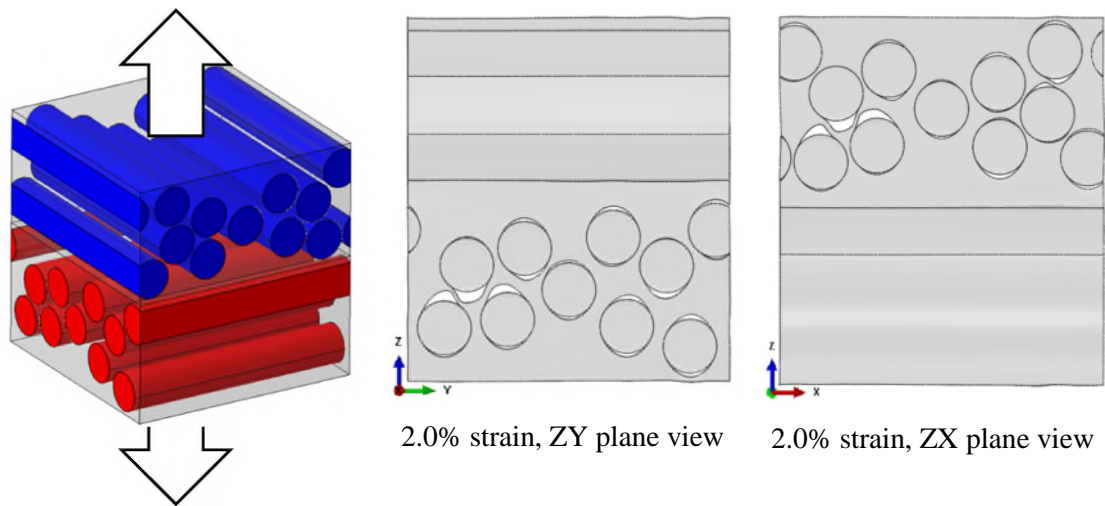

2.0% strain, ZY plane view   2.0% strain, ZX plane view

Figure 11: Loading scenario and scaled deformed shape of 0°/ 90° laminate in tension, showing the failed cohesive interfaces

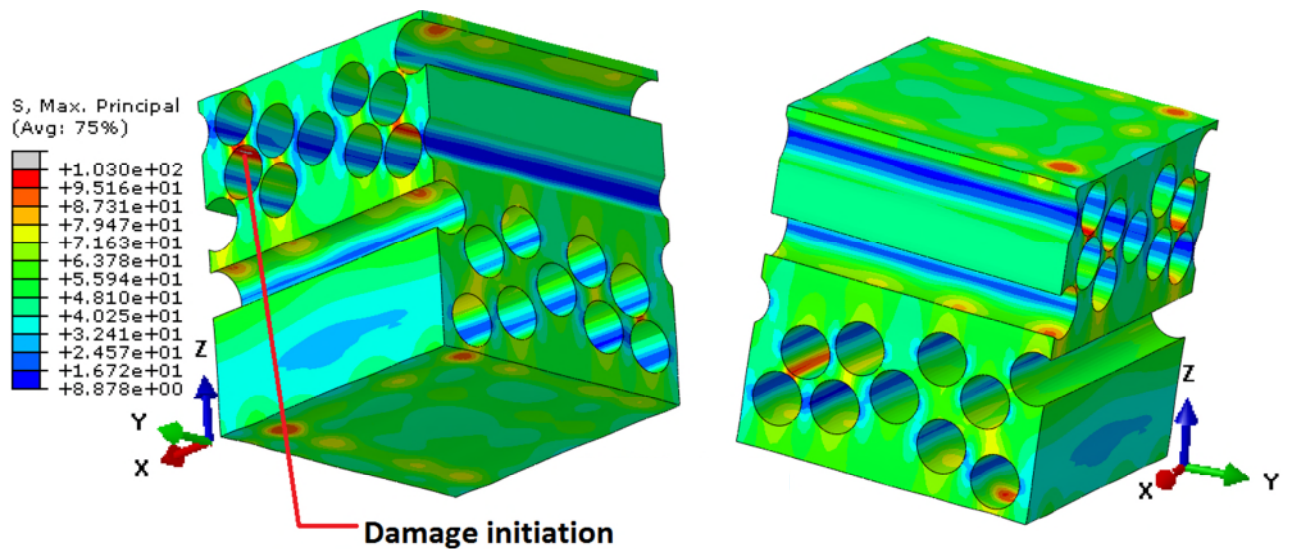*Figure 12:* Maximum principle stress fringe plot of the 0°/ 90° laminate in tension, indicating the location of damage initiation at 0.6% tension strain.

Similarly to the above multidirectional layup and loading scenario, all the loading scenarios shown in figure 5 were investigated and the resulting damage initiation strengths are tabulated on table 4.Unlike the unidirectional scenarios shown in figures 6 to 10, in the multidirectional ply arrangements it was observed on the stress plots that a true three-dimensional stress state occurred. The two plies with different orientations were influencing each other's stress state. Smaller high-stress areas can be observed along each fibre, as an effect of the remote cross-fibres in the other lamina. The effect of this can also be observed on the top and bottom faces of the RVE due to the symmetric boundary conditions.

Table 4: RVE failure initiation strength

Orientations	Mode I (MPa)	Mode II (MPa)
0°/0°	38.03	54.17
0°/45°	46.83	36.88
0°/90°	52.93	41.46
±45°	52.93	38.41
90°/90°	38.03	37.67
90°/45°	46.83	23.09

5. Conclusions

In the previous sections, nine separate micromechanical models were presented to determine the failure imitation strength between two unidirectional FRP laminas of different orientations, under mode I and mode II loading. Damage at the micromechanical level was initiated either at the fibre-matrix interface region following the fracture toughness values dictated and according to the BK mixed mode failure law, or in the form of yield initiation on the matrix. The locations in the models were damage was initiated following wither failure modes, was governed by the proximity between the fibres in a lamina. No damage was observed in the resin rich matrix region in between two laminas of the same or different orientation.

The study provided with evidence, for the material properties and modelling assumptions used, that traction separation modelling laws in regards to the failure initiation i.e. the cohesive strength, depend on the orientation of the laminas forming the interface. Currently, this result is not accounted for when modelling delamination with traction separation laws.

Damage initiation in multidirectional laminates under mode I opening displacement was observed at higher stress levels for larger differences in the lamina orientations. The lowest value was found for the case of longitudinal unidirectional laminate and the maximum in the case of longitudinal/transverse cross plies, while the results obtained for the 0°/45° layup was in between.

For the case of mode II strength, damage initiation pattern varied. The strength was higher when a longitudinal ply was present due to the fact that the longitudinal out of plane shear strength in composites was higher than the transverse shear strength. However, the 0°/45° case was an exception, as it provided a slightly lower strength than the 90°/90° case which can be attributed to numerical inaccuracies and to the statistical nature in the fibre distributions. The strength obtained for the case of the 90°/45° laminate showed a significantly lower value than that for the other layups effect that could be attributed to the presence of the low shear-strength transverse ply combined with the effect of the 45° fibres

on the stress states, creating high-stress areas inside the matrix at much lower global loads than in other configurations.

Acknowledgements

References

[1] McCarthy CT, Vaughan T. Micromechanical failure analysis of advanced composite materials. In: Camanho PP, Hallett SR, editors. Numerical Modelling of Failure in Advanced Composite Materials. Cambridge: Woodhead publishing; 2015, p. 379–409.

[2] Vaughan TJ, McCarthy CT. A combined experimental-numerical approach for generating statistically equivalent fibre distributions for high strength laminated composite materials. Compos Sci Technol 2010;70:291–7

[3] Trias D, Costa J, Turon A, Hurtado JE. Determination of the critical size of a statistical representative volume element (SRVE) for carbon reinforced polymers. Acta Mater 2006;54:3471–84

[4] Gonzalez C, LLorca J. Mechanical behavior of unidirectional fiber-reinforced polymers under transverse compression: Microscopic mechanisms and modeling. Compos Sci Technol 2007;67:2795–806

[5] O'Dwyer DJ, O'Dowd NP, McCarthy CT. Numerical micromechanical investigation of interfacial strength parameters in a carbon fibre composite material. J Compos Mater 2013;48:749–60.

[6] Digimat software 2016. http://www.e-xstream.com/products/digimat/about-digimat

[7] Abaqus-Inc. Abaqus 6.14 - Getting Started with Abaqus. Province: RI: Dassault Systèmes Simulia Corp.; 2014.

[8] Hojo M, Ando T, Tanaka M, Adachi T, Ochiai S, Endo Y. Modes I and II interlaminar fracture toughness and fatigue delamination of CF/epoxy laminates with self-same epoxy interleaf. Int J Fatigue 2006;28:1154–65

[9] Vaughan TJ, McCarthy CT. Micromechanical modelling of the transverse damage behaviour in fibre reinforced composites. Compos Sci Technol 2011;71:388–96

[10] Arteiro A, Catalanotti G, Melro AR, Linde P, Camanho PP. Micro-mechanical analysis of the in situ effect in polymer composite laminates. Compos Struct 2014;116:827–40.

[11] Benzeggagh ML, Kenane M. Measurement of mixed-mode delamination fracture toughness of unidirectional glass/epoxy composites with mixed-mode bending apparatus. Compos Sci Technol 1996;56:439–49